Fuel Cell Basics

Hydrogen Energy. Edited by Detlef Stolten

ISBN: 978-3-527-32711-9

1
Electrocatalysis and Catalyst Degradation Challenges in Proton Exchange Membrane Fuel Cells

Hubert A. Gasteiger, Daniel R. Baker, Robert N. Carter, Wenbin Gu, Yuxin Liu, Frederick T. Wagner, and Paul T. Yu

Abstract

After a brief review of the kinetics of the cathodic oxygen reduction and the anodic hydrogen oxidation reaction, a fundamental membrane electrode assembly performance model is outlined, which demonstrates that a 4–10-fold reduced amount of platinum is required for commercially viable large-scale vehicle applications. The various catalyst technology roadmaps to achieve this goal are discussed. With the increasing number of prototype proton exchange membrane fuel cell (PEMFC)-powered vehicles, catalyst durability has also become a strong focus of academic and industrial R&D. Therefore, the key issues of platinum sintering/dissolution under dynamic vehicle operation and of carbon-support corrosion during PEMFC startup/shutdown are reviewed.

Keywords: electrocatalysis, platinum catalysts, catalyst degradation, carbon-support corrosion, proton exchange membrane fuel cells, fuel cell-powered vehicles, hydrogen oxidation

1.1
Introduction

Over the past few years, significant R&D efforts have been aimed at meeting the challenging performance and cost targets for the use of proton exchange (PEM) fuel cells in vehicles. Catalyst development and optimization of membrane electrode assemblies (MEAs) increased PEM fuel cell power densities to levels which satisfy vehicle packaging needs ($\sim 1\,\mathrm{W\,cm^{-2}}$) at platinum catalyst loadings of $\sim 0.5\,\mathrm{mg_{Pt}\,cm^{-2}_{MEA}}$, corresponding to Pt specific power densities of $\sim 0.5\,\mathrm{g_{Pt}\,kW^{-1}}$, which equates to ~ 50 g of platinum in a 100 kW automotive fuel cell stack [1]. This, together with the development of high-pressure hydrogen tanks (70 MPa), permitted the construction of small fuel cell vehicle test fleets for testing under real driving conditions, leading to the demonstration by Toyota and General Motors that a vehicle driving range of 300 miles can indeed be met. However, as shown in an ongoing study by the United States Depart-

Hydrogen Energy. Edited by Detlef Stolten

ISBN: 978-3-527-32711-9

ment of Energy (DoE), conducted by the National Renewable Energy Laboratory (NREL), the durability of a significant number of fuel cell vehicles from various companies averages only 1200 h (with a maximum of 1900 h), limited mostly by catalyst degradation [2]. Therefore, irrespective of the questions regarding the viability of the future generation of renewable hydrogen and the infrastructure required for its distribution, large-scale commercialization of PEM fuel cell vehicles still requires significant advances in catalyst development in order both to reduce the amount of platinum metals required to run a fuel cell stack and to enhance catalyst durability. Approaches to how one might reach the catalyst activity target of $<0.2\ g_{Pt}\,kW^{-1}$ [1] and the underlying degradation phenomena which currently limit PEM fuel cell life in vehicles to significantly less than the 6000 h life target are discussed in this chapter.

1.2 Voltage Losses in State-of-the-Art Automotive PEM Fuel Cells

In order to determine whether a reduction in the platinum specific power density below the current value of $\sim 0.5\ g_{Pt}\,kW^{-1}$ can be achieved by further optimization of electrode, diffusion medium (DM) and MEA structures, the value of the various voltage loss terms in state-of-the-art MEAs must be quantified. Therefore, over many years, work at General Motors has been focused on developing methods by which the voltage losses due to catalyst kinetics and various transport processes in an MEA could be predicted on the basis of fundamental physical-chemical parameters, in order to provide a model of the cell voltage, E_{cell}, as a function of current density, i:

$$E_{cell} = E_{rev.} - i \times (R_{electronic} + R_{membrane}) - \eta_{HOR} - |\eta_{ORR}| - i \times R_{H^+,\,eff.} - \eta_{tx,\,gas\,(dry)} - \eta_{tx,\,gas\,(wet)} \quad (1.1)$$

where $E_{rev.}$ is the reversible thermodynamic potential depending on temperature and gas partial pressure and $R_{electronic}$ are the electronic resistances in an MEA (mostly the contact resistance between the DM and the bipolar plate flow-field [3]). Whereas these terms are independent of current density, all other terms vary with current density: $R_{membrane}$ is the relative humidity (RH)-dependent proton conduction resistance of the membrane [4], η_{HOR} is the overpotential loss for the hydrogen oxidation reaction (HOR) [5], η_{ORR} is the overpotential loss for the oxygen reduction reaction (OOR) [3], $R_{H^+,\,eff.}$ is the effective RH-dependent proton conduction resistance in the anode and the cathode electrode [6, 7], $\eta_{tx,\,gas\,(dry)}$ is the gas diffusion overpotential mostly controlled by the diffusion of oxygen in air through the diffusion medium and the cathode electrode in the absence of liquid water (in the case of PEM fuel cell operation with pure hydrogen, voltage losses from hydrogen diffusion are essentially negligible) [8], and $\eta_{tx,\,gas\,(wet)}$ are additional gas diffusion overpotential losses caused by the presence of liquid water in the diffusion media and the electrodes.

Using independently measured physical-chemical parameters for the various terms in Equation 1.1, a quasi-two-dimensional down-the-channel model was developed (normal to the MEA surface and along the flow-field channel) to describe the various voltage loss terms as a function of current density for typical automotive operating conditions. This is shown in Figure 1.1, illustrating the well-known fact that the slow ORR kinetics on a state-of-the-art carbon-supported platinum catalyst (Pt/C) are responsible for about two-thirds of the overall voltage losses at high current density, evidenced by comparing the ORR kinetics-limited performance (top line in Figure 1.1) with the actual performance of a full active area PEM fuel cell short-stack (lowest line in Figure 1.1, with error bars indicating the standard deviation in cell voltage for all MEAs in the stack). The voltage losses due to the hydrogen oxidation reaction at the anode are negligible under the conditions shown in Figure 1.1 ($\ll 5$ mV at 1.5 A cm^{-2}) [5, 8]. The ohmic losses at the highest current density of 1.5 A cm^{-2} are ~ 90 mV and are mostly due to electronic contact resistances (~ 60 mV), with only ~ 30 mV losses caused by the proton conduction resistance of the membrane; clearly, the development of low-resistance bonding between the bipolar plate flow-field and the diffusion medium could result in up to 5% efficiency gains at 1.5 A cm^{-2}. The remaining voltage loss terms from proton conduction resistances in the electrodes and from oxygen diffusion resistances through a nominally dry diffusion medium and electrode are small, adding up to only ~ 40 mV at 1.5 A cm^{-2}. It should be mentioned that the last term in Equation 1.1 cannot be determined from measurable materials properties and thus represents the difference between the predicted losses (short dashed line in Figure 1.1) and the measured cell voltage (lowest line in Figure 1.1). The reason why this difference is very small (~ 20 mV at 1.5 A cm^{-2}) is that the maximum local RH in the MEA barely reaches 100% at the highest current density [8], so that blocking of electrode and DM pores by liquid water is not a strong factor under automotive operating conditions characterized by low RH conditions for reasons of systems simplification [9]. It should be noted that the model predictions shown in Figure 1.1 are consistent with the measured high-frequency resistance and were also validated by comparing the predicted current distribution along the flow-field channels with current distribution measurements in full active area hardware [8].

Given the fact that the voltage losses due to electronic, proton, and gas transport resistances are rather small, it is clear that significant increases in the platinum specific power density can only be achieved by reducing the catalyst loadings on both the anode and the cathode electrode. This, however, would lead to lower cell voltages and therefore to lower fuel cell efficiencies, which cannot be tolerated as it would sacrifice the promised high energy efficiency of fuel cell vehicles and would also lead to additional engineering challenges with regards to heat rejection via the vehicle radiator [9].

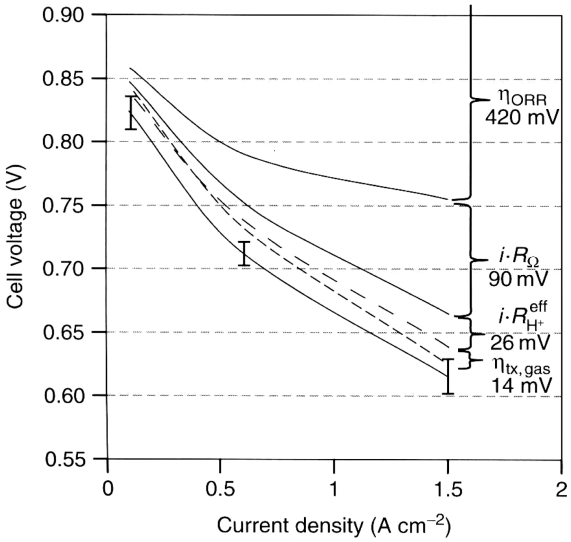

Fig. 1.1 Voltage loss terms in state-of-the-art H_2-air PEM fuel cell full active area short-stack (~20 cells) operated under representative automotive conditions. MEAs: 0.2/0.3 $mg_{Pt}\,cm^{-2}$ (anode/cathode) coated on an 18 μm thick perfluorosulfonic acid membrane and sandwiched between 200 μm thick diffusion media (SGL 25BC) on both the anode and cathode sides. Operating conditions vary with current density: (i) at low current density, P_{inlet} = 110 kPa_a, $T_{coolant,\,out}$ = 72 °C, RH_{inlet} = 30/45% (anode/cathode), and H_2-air feeds at s = 2/5.5 (anode/cathode); (ii) at high current density, P_{inlet} = 155 ± 20 kPa_a, $T_{coolant,\,out}$ = 80 °C, RH_{inlet} ~ 30/60% (anode/cathode), and H_2-air feeds at s = 2/1.8 (anode/cathode). For details, see [8]. Reproduced from W. Gu *et al.* [8], with permission from John Wiley & Sons, Ltd.

1.3 Catalyst Development Needs and Approaches

Based on the above-outlined considerations, either non-platinum catalysts or more active platinum-based catalysts must be developed, so that the required amount of platinum can be reduced without loss of power density and efficiency. Although significant advances have been made in the area of non-Pt cathode catalysts [10], Pt-based catalysts are currently still the most promising option to provide the high power densities required for vehicle applications. The activity gains that would have to be realized by advanced platinum-based catalysts in order to lower the Pt specific power densities are shown in Table 1.1, considering that the platinum loadings on the anode electrode can be lowered to 0.05 $mg_{Pt}\,cm^{-2}$ without losses in fuel cell performance in the case of fuel cell operation with pure hydrogen [5].

Table 1.1 shows that the total amount of Pt in the MEA can be reduced significantly without performance loss by lowering the anode Pt loading and by implementation of carbon-supported Pt-alloy catalysts (e.g., Pt_3Co/C [1, 11]) with

Table 1.1 Effect of lowering platinum loadings on the anode (L_{anode}) and the cathode ($L_{cathode}$) on the platinum specific power density, P_{Pt}, by assuming that the current high current density performance of the MEA can be maintained at the level shown in Figure 1.1 (i.e., 0.62 V at 1.5 A cm^{-2}, corresponding to 0.93 W cm^{-2}): this requires advanced cathode catalysts for the ORR which have improved mass activity over currently used state-of-the-art Pt/C.

L_{anode} (mg_{Pt} cm^{-2})	$L_{cathode}$ (mg_{Pt} cm^{-2})	P_{Pt} (g_{Pt} kW^{-1})	Cathode catalyst technology
0.20	0.30	0.54	Conventional Pt/C, see Figure 1.1
0.05	0.20	0.27	"2×" conventional Pt alloy/C
0.05	0.10	0.16	"4×" Pt-based cathode catalyst
0.05	0.05	0.10	"10×" Pt-based cathode catalyst

demonstrated close to twofold higher *Pt mass activity* (in units of A mg_{Pt}^{-1} at a given potential; see below) compared with Pt/C. Implementation of this near-term "2×" cathode catalyst technology is expected to lead to Pt specific power densities of $P_{Pt} \sim 0.27\ g_{Pt}\ kW^{-1}$, closely approaching the initially announced target of $<0.2\ g_{Pt}\ kW^{-1}$ [1]. Conceptually, the latter can be reached by the recently developed *dealloyed Pt alloy* catalysts (third row in Table 1.1), which have shown fourfold higher mass activities compared with Pt/C [12, 13]. Although this concept must still be proven for its long-term stability in operating PEM fuel cells, it is a promising path towards reaching the initial $<0.2\ g_{Pt}\ kW^{-1}$ goal. However, considering the significant constraint on world-wide platinum resources, large-scale PEM fuel cell vehicle commercialization really necessitates a reduction in the platinum content per vehicle to the order to 10 g_{Pt}, i.e., $P_{Pt} \sim 0.1\ g_{Pt}\ kW^{-1}$ for a 100 kW PEM fuel cell vehicle. As shown in Table 1.1 (bottom row), this would require novel Pt-based cathode catalysts with 10-fold higher mass activity compared with conventional Pt/C.

In principle, there are two possible pathways towards platinum-based cathode catalysts with "10×" higher Pt mass activity, $i_{m(0.9\ V)}$ (in A mg_{Pt}^{-1}), which is commonly defined at a potential of 0.9 V versus the reversible hydrogen electrode (RHE) potential at an oxygen partial pressure of 100 kPa_a [3]. This is best illustrated by considering that the Pt mass activity for the ORR depends on both the *specific activity* of a Pt-based catalyst, $i_{s(0.9\ V)}$ (in μA cm_{Pt}^{-2}), and its specific surface area, A_{Pt} (in $m_{Pt}^2\ g_{Pt}^{-1}$):

$$i_{m(0.9\,V)}[A\ mg_{Pt}^{-1}] = i_{s(0.9\,V)}[\mu A\ cm_{Pt}^{-2}] \times A_{Pt}[m_{Pt}^2\ g_{Pt}^{-1}] \times 10^{-5} \quad (1.2)$$

where the specific activity represents the intrinsic activity of a platinum catalyst surface (directly proportional to the so-called turnover frequency in heterogeneous catalysis), while the specific surface area is a measure of the exposed

platinum surface area per unit platinum mass (also referred to as platinum dispersion). Hence there are two different pathways to increase platinum mass activity, via [14]: (i) core-shell concepts where a platinum monolayer is supported on a non-platinum nanoparticle leading to very high platinum specific surface areas and, consequently, to high mass activity [15] and also ultra-thin platinum (alloy) coatings supported on nanostructured supports [16]; and/or (ii) increased specific activity through alloying of platinum with transition metals [12, 17, 18], or the extraordinarily high specific activity observed for the (111) surface planes of Pt alloys [17, 19].

Figure 1.2a shows the specific activity gains observed for polycrystalline bulk platinum alloys, with Pt_3Co, Pt_3Ni, and Pt_3Fe yielding two- to threefold higher specific activity over pure platinum, consistent with what was observed for high surface area carbon-supported Pt alloys [1, 11, 20]. Specific activities depend not only on the actual transition metal, but also on the surface structure of the Pt alloy [17]: (i) *skeleton* structures are produced by removal of the acid-soluble transition metal from the Pt alloy surface during acid leaching or contact with the acidic electrolyte (aqueous or ionomeric); (ii) *Pt skin* structures are produced by platinum surface segregation during high-temperature annealing in vacuum or inert gas. It was shown recently that the same structures and a similar effect on specific activity are observed for high surface area carbon-supported Pt alloy catalysts [21].

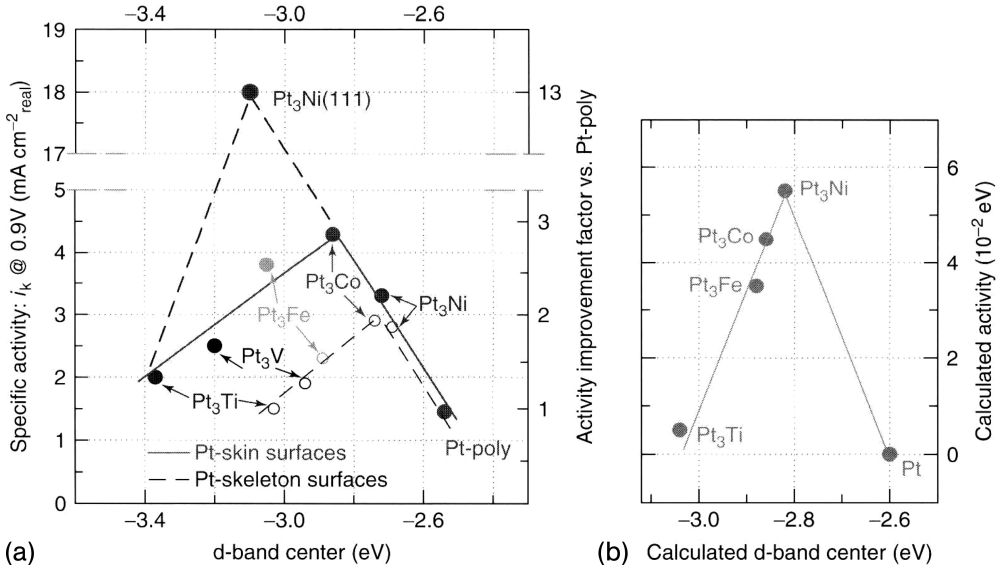

Fig. 1.2 Relationship between experimentally measured specific activities for the ORR on Pt_3M surfaces in 0.1 M $HClO_4$ at 0.9 V versus RHE and 60 °C versus the d-band center position. (a) Experimental specific activities, $i_{s(0.9\ V)}$, for Pt alloy skin and skeleton type surfaces. (b) Activities and d-band center positions calculated by DFT for (111) oriented skin surfaces. Reproduced from V. R. Stamenkovic and N.M. Markovic [17], with permission from John Wiley & Sons, Ltd.

In addition, Figure 1.2a also shows the extraordinarily high specific activity observed for the (111) surface planes of $Pt_3Ni(111)$ single crystals [17, 19]. As shown in Figure 1.2b, the activity enhancement by alloying of Pt with transition metals can be understood on the basis of *ab initio* density functional theory (DFT) molecular models, which relate the transition metal-induced shift of the d-band center energy with the binding strength of adsorbed oxygen intermediates, thereby affecting the oxygen reduction activity [18, 22]. While the alloying-induced variation in specific activity for the ORR is well described by DFT (see Figure 1.2b), the large differences observed between various low-index surface planes of Pt skin-terminated Pt_3Ni single crystals has been surprising, showing roughly four- and eightfold higher specific activity of $Pt_3Ni(111)$ compared with $Pt_3Ni(110)$ and $Pt_3Ni(100)$, respectively [19]. Even though these activities were measured in aqueous perchloric acid electrolyte using the rotating disk electrode (RDE) method, it was shown in the past that the activity of carbon-supported Pt and Pt alloy catalysts obtained by RDE measurements is in good quantitative agreement with their ORR activity in MEAs tested in fuel cells under comparable conditions [1, 23].

Considering the excellent correspondence between ORR activities measured in MEAs and by RDE in conjunction with the extremely high specific activity obtained on $Pt_3Ni(111)$ surfaces, it is tempting to raise the question of whether one could envision its incorporation into MEAs. One possibility would be the shape-controlled synthesis of *large-nano* octahedral Pt_3Ni particles which would be terminated by (111) surface planes [14], similarly to what had been demonstrated for Pt_3Fe alloys [24]. In this case, however, the size of the Pt_3Ni octahedra would have to be large in order to provide large enough (111) surface planes which then might exhibit the same high specific activity as that found on bulk $Pt_3Ni(111)$ single crystals. Based on Equation 1.1, however, the low platinum specific surface area, A_{Pt}, of large-nano octahedra would compromise the achievable mass activity, which of course is the ultimate figure of merit for catalyst activity in fuel cells. The latter may be estimated using Equation 1.1 in combination with the measured specific activity of $i_{s(0.9\ V)} = 18\,000\ \mu A\ cm_{Pt}^{-2}$ for $Pt_3Ni(111)$ (see Figure 1.2a) and the approximate platinum specific surface area of $A_{Pt} \sim 250\ m_{Pt}^2\ g_{Pt}^{-1} \times (d_{Pt_3Ni}\,[nm])^{-1}$ based on simple geometric arguments. The results are shown in Figure 1.3.

Clearly, Figure 1.3 suggests that the mass activity even of 30 nm large Pt_3Ni octahedra would be 10 times larger than that of a state-of-the-art Pt/C catalyst [$i_{m(0.9\ V)} = 0.16\ A\ mg_{Pt}^{-1}$] [14], corresponding to the long sought for "10×" ORR catalyst mentioned in Table 1.1. The future will show whether this concept can indeed be realized, in which case one of the major hurdles for fuel cell commercialization could be resolved.

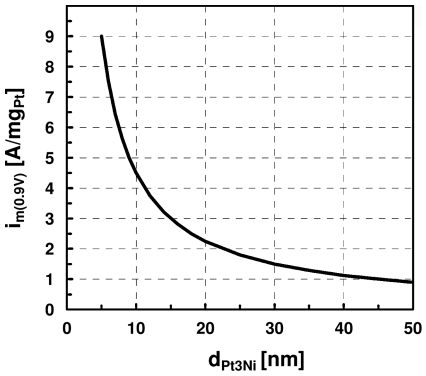

Fig. 1.3 Projected Pt mass activity versus particle diameter for Pt_3Ni octahedra exposing (111) facets, assuming no effect of (111) terrace width on activity.

1.4 Catalyst Degradation via Platinum Dissolution

Catalyst degradation in operating PEM fuel cells occurs mostly under transient conditions, leading both to dissolution of the active catalyst components (i.e., Pt and Pt alloys) [25–27]) and also to carbon-support corrosion (i.e., decomposition into CO_2) [28, 29]. The former is caused by the finite solubility of platinum at the cathode potentials in acidic electrolytes [25], particularly under voltage-cycling conditions (produced by power or load cycling under vehicle operation) [30, 31], since the formation of more dissolution-resistant platinum oxide is a kinetically slow process [32]. Platinum dissolution leads to a loss of active surface area during extended voltage cycling by two different mechanisms [25]: (i) diffusion of dissolved platinum species towards the membrane and platinum precipitation in the membrane phase due to reaction with hydrogen permeating through the membrane from the anode side, leading to a loss of electrically connected platinum surface area; and (ii) Ostwald ripening of platinum inside the cathode electrode, particularly near the cathode/DM interface, leading to a loss of platinum surface area due to nanoparticle growth. The same phenomenon is observed with Pt alloys, with the difference that the dissolved transition metals will remain in the ionomer phase as their reduction potential is below that of hydrogen [26]; if significant amounts of transition metal are dissolved, fuel cell performance is compromised, particularly at high current densities [33]. Since platinum nanoparticle solubility decreases with increasing particle size, following the Gibbs-Thomson relationship, larger particles are more stable towards voltage cycling [34, 35], which gives some hope that large-nano Pt alloys might display improved durability in addition to improved ORR activity [14].

Unfortunately, platinum surface area loss leads to a decrease in platinum mass activity, particularly during voltage cycling. This is shown in Figure 1.4, where 30 000 accelerated voltage cycles lead to a two- to threefold loss in mass activity in the case of both pure platinum and Pt alloy catalysts. Nevertheless, the mass activity advantage of Pt alloys of over pure Pt is maintained during

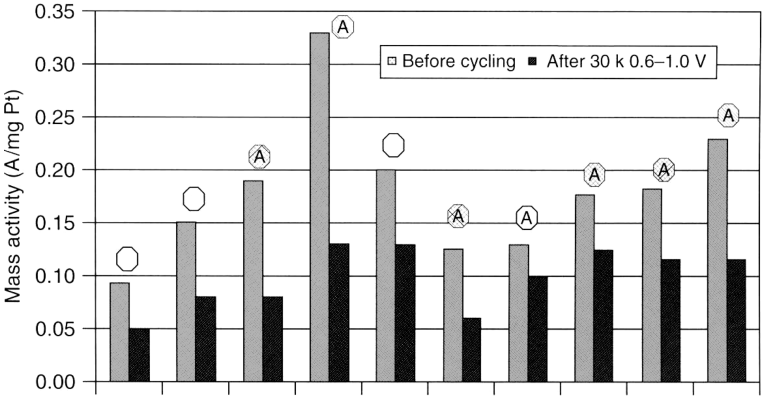

Fig. 1.4 Mass activity, $i_{m(0.9\,V)}$, of Pt/C (symbols without letter) and Pt alloy/C (symbols with letter A) before and after 30 000 voltage-cycles between 0.6 and 1.0 V RHE at 20 mV s^{-1} in H_2–N_2 (counterelectrode/cathode electrode) at 80 °C, 100% RH, and ambient pressure. Open symbols represent conventional carbon supports (e.g., Vulcan XC72, Ketjen black), shaded symbols with a crossing line represent fully graphitized carbon supports, and shaded symbols without a crossing line are acetylene blacks. Reproduced from F.T. Wagner *et al.* [36], with permission from John Wiley & Sons, Ltd.

these experiments; similar behavior was observed for dealloyed Pt-Cu/C catalysts [13]. Owing to the strongly degrading effect of voltage cycling, automotive fuel cell systems are generally hybridized with batteries to reduce the number of voltage cycles during fuel cell operation.

1.5 Carbon-Support Corrosion

Under steady-state fuel cell operation, carbon-support corrosion is a minor contributor to voltage degradation. However, carbon-support corrosion is significantly accelerated during start/stop cycles, due to the simultaneous but spatially separated presence of hydrogen and oxygen (air) in the anode flow field, forming a so-called hydrogen-air front: (i) when stopping a fuel cell system, the hydrogen supply to the anode is turned off, and air will leak slowly into the anode compartment; (ii) after a long shut-down, the anode compartment will be filled with air via leaks to the environment, which will be replaced by hydrogen when starting the fuel cell. This effect was first discussed by Reiser *et al.* [29], and is depicted in Figure 1.5.

Owing to the high electronic conductivity of the bipolar plates, hydrogen electrooxidation in the anode compartment (lower left corner of Figure 1.5) leads to the reduction of spatially separated oxygen in the anode compartment (upper left corner of Figure 1.5). Since the effective proton conduction resistance along the proton-conducting membrane is very high over millimeter length distances, the protons for the oxygen reduction reaction in the anode compartment are

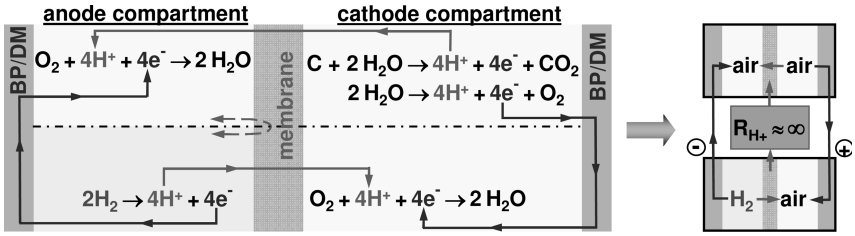

Fig. 1.5 Schematics of the processes leading to carbon-support corrosion during either fuel cell start/stop transients or during local hydrogen starvation. The simultaneous presence of spatially separated regions of hydrogen and oxygen (from air) on the anode side effectively leads to the phenomenon that an H_2–air fuel cell drives a current through an air–air electrolytic cell (see the right-hand side).

supplied by the opposing cathode compartment, leading to an increase in the local cathode potential until oxygen evolution or carbon corrosion occurs. This can be understood more easily by the sketch on the right-hand side of Figure 1.5, conceptually splitting the stack into an H_2-air fuel cell (lower part) which is electrically short-circuited with an electrolytically driven air-air cell. Using the known kinetics for the various reactions (HOR, ORR, oxygen evolution, and carbon corrosion), the start/stop-induced carbon-support corrosion rates can be modeled very accurately [28, 29, 37–39].

An analysis of the detailed start/stop mechanism shows that its effect can be mitigated by both materials and systems solutions. Of course, the most straightforward mitigation strategy is to minimize the residence time of the H_2-air front in the anode compartment, which can be done most effectively for the startup procedure [28, 38]; other system controls-related mitigation strategies were discussed in detail by Perry *et al.* [40]. On the materials side, start/stop degradation can be reduced by replacing conventional carbon supports (e.g., Vulcan XC72 or Ketjen black) with either acetylene blacks or fully graphitized carbon supports [28, 38]. Also, since the rate of oxygen reduction in the anode compartment determines the rate of carbon corrosion on the opposing cathode electrode, lowering of the platinum loading on the anode electrode leads to lower start/stop degradation, one of the rare instances where lowering the platinum loading actually improves durability without affecting performance due to the very high HOR activity of Pt/C [5].

The phenomenon of localized hydrogen starvation is closely related to that of start/stop degradation. In the former, oxygen permeation through the membrane from the cathode side in regions of the anode flow field with poor or interrupted hydrogen supply (e.g., by water droplets blocking anode flow field channels) again leads to oxygen reduction on the anode and to an increase in the local cathode potential to where carbon corrosion can occur [28, 39, 41]. Compared with start/stop degradation, the degradation rates are slower in this case, since carbon corrosion rates are limited by the permeation rate of oxygen through the membrane [28]. The materials-related mitigation strategies, naturally, are the same as in the case of start/stop degradation [28].

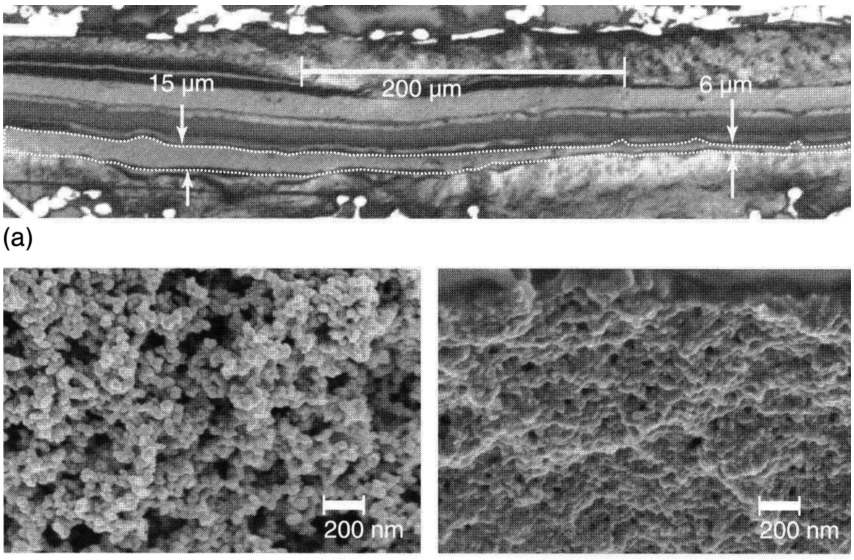

Fig. 1.6 (a) Optical micrograph showing the cross-section of an aged MEA (mounted in epoxy) that spans regions that were starved (right-hand side) and not starved (left-hand side) of hydrogen. The cathode electrode is outlined with dotted white lines for clarity. Scanning electron micrograph (SEM) images of freeze-fractured sections of the MEA showing the cathode electrode from different regions of the MEA: (b) cathode electrode after aging in the non-starved region; (c) cathode electrode after aging in the H_2-starved region. Note that SEM analysis was done on separate samples that were not mounted in epoxy. Reproduced from R.N. Carter *et al.* [37], with permission from John Wiley & Sons, Ltd.

Voltage losses from start/stop degradation or local hydrogen starvation are most apparent at high current densities [38], pointing to increased mass transport resistances. This can be understood by the observation that the associated carbon-support corrosion leads to so-called *cathode thinning*, caused by a loss of cathode electrode void volume, which in turn increases oxygen diffusion resistances. This is illustrated in Figure 1.6, showing the thinning of the cathode electrode over hydrogen-starved regions of the anode flow field (a), leading to a loss of cathode electrode void volume in the thinned regions (c) compared with the non-corroded regions (b).

Considering the rapid degradation which can be produced by H_2-air fronts occurring during fuel cell startup and shutdown processes, leading to unacceptably large performance losses after only 100 slow H_2-air front events [38], it becomes apparent that the fuel cell control system must be extremely rugged to permit long-term durability. Although this can be approached at the systems design level, it would of course be desirable in the long term to develop and implement more durable cathode catalyst support materials based on graphitized carbon supports or more resistant non-carbon supports such as the nanostruc-

tured supports developed by 3M [16]. Alternatively, anode catalysts which have no activity for the oxygen reduction reaction would provide a materials-based solution to improve start/stop robustness.

1.6 Conclusion

The current major challenges for developing commercially viable PEM fuel cell vehicles are the need to lower the platinum loading of the MEA without loss of performance and to improve the stability of the catalyst with respect to platinum dissolution and carbon-support corrosion. Based on catalyst development advances in the past few years, several promising concepts exist, which might eventually permit commercially viable platinum loadings [dealloyed Pt alloys, thin Pt (alloy) films on nanostructured supports, large-nano shape-controlled Pt alloys]. Start/stop degradation can to a large extent be mitigated by system controls, but advanced support and catalyst materials to improve system robustness are desired.

References

1 Gasteiger, H.A., Kocha, S.S., Sompalli, B., and Wagner, F.T. (2005) *Appl. Catal. B*, **56**, 9.

2 Wipke, K., Sprik, S., Kurtz, J., and Garbak, J. (2009) Field experience with fuel cell vehicles. In *Handbook of Fuel Cells – Fundamentals, Technology and Applications* (eds W. Vielstich, H.A. Gasteiger, and H. Yokokawa), John Wiley & Sons, Ltd, Chichester, vol. 6, p. 893.

3 Neyerlin, K.C., Gu, W.B., Jorne, J., and Gasteiger, H.A. (2006) *J. Electrochem. Soc.*, **153**, A1955.

4 Mittelsteadt, C.K. and Liu, H. (2009) Conductivity, permeability, and ohmic shorting of ionomeric membranes. In *Handbook of Fuel Cells – Fundamentals, Technology and Applications* (eds W. Vielstich, H.A. Gasteiger, and H. Yokokawa), John Wiley & Sons, Ltd, Chichester, vol. 5, p. 345.

5 Neyerlin, K.C., Gu, W.B., Jorne, J., and Gasteiger, H.A. (2007) *J. Electrochem. Soc.*, **154**, B631.

6 Neyerlin, K.C., Gu, W., Jorne, J., Clark, A., and Gasteiger, H.A. (2007) *J. Electrochem. Soc.*, **154**, B279.

7 Liu, Y.X., Murphy, M.W., Baker, D.R., Gu, W.B., Ji, C.C., Jorne, J., and Gasteiger, H.A. (2009) *J. Electrochem. Soc.*, **156**, B970.

8 Gu, W., Baker, D.R., Liu, Y., and Gasteiger, H.A. (2009) Proton exchange membrane fuel cell (PEMFC) down-the-channel performance model. In *Handbook of Fuel Cells – Fundamentals, Technology and Applications* (eds W. Vielstich, H.A. Gasteiger, and H. Yokokawa), John Wiley & Sons, Ltd, Chichester, vol. 6, p. 631.

9 Masten, D.A. and Bosco, A.D. (2003) System design for vehicle applications. In *Handbook of Fuel Cells – Fundamentals, Technology and Applications* (eds W. Vielstich, A. Lamm, and H.A. Gasteiger), John Wiley & Sons, Ltd, Chichester, vol. 3, p. 714.

10 Lefevre, M., Proietti, E., Jaouen, F., and Dodelet, J.-P. (2009) *Science*, **324**, 71.

11 Yu, P., Pemberton, M., and Plasse, P. (2005) *J. Power Sources*, **144**, 11.

12 Mani, P., Srivastava, R., and Strasser, P. (2008) *J. Phys. Chem. C*, **112**, 2770.

13 Neyerlin, K.C., Srivastava, R., Yu, C.F., and Strasser, P. (2009) *J. Power Sources*, **186**, 261.

14 Gasteiger, H.A. and Markovic, N.M. (2009) *Science*, **324**, 48.

15 Adzic, R.R., Zhang, J., Sasaki, K., Vukmirovic, M.B., Shao, M., Wang, J.X., Nilekar, A.U., Mavrikakis, M., Valerio, J.A., and Uribe, F. (2007) *Top. Catal.*, **46**, 249.

16 Debe, M.K., Schmoeckel, A.K., Vernstrorn, G.D., and Atanasoski, R. (2006) *J. Power Sources*, **161**, 1002.

17 Stamenkovic, V.R. and Markovic, N.M. (2009) Oxygen reduction on platinum bimetallic alloy catalysts. In *Handbook of Fuel Cells – Fundamentals, Technology and Applications* (eds W. Vielstich, H.A. Gasteiger, and H. Yokokawa), John Wiley & Sons, Ltd, Chichester, vol. 5, p. 18.

18 Greeley, J., Stephens, I.E.L., Bondarenko, A.S., Johansson, T.P., Hansen, H.A., Jaramillo, T.F., Rossmeisl, J., Chorkendorff, I., and Norskov, J.K. (2009) *Nat. Chem.*, **1**, 552.

19 Stamenkovic, V.R., Fowler, B., Mun, B.S., Wang, G.F., Ross, P.N., Lucas, C.A., and Markovic, N.M. (2007) *Science*, **315**, 493.

20 Thompsett, D. (2003) Platinum alloys as oxygen reduction catalysts. In *Handbook of Fuel Cells – Fundamentals, Technology and Applications* (eds W. Vielstich, A. Lamm, and H.A. Gasteiger), John Wiley & Sons, Ltd, Chichester, vol. 3, p. 467.

21 Chen, S., Sheng, W., Yabuuchi, N., Ferreira, P.J., Allard, L.F., and Shao-Horn, Y. (2009) *J. Phys. Chem. C*, **113**, 1109.

22 Stamenkovic, V., Mun, B.S., Mayrhofer, K.J.J., Ross, P.N., Markovic, N.M., Rossmeisl, J., Greeley, J., and Norskov, J.K. (2006) *Angew. Chem. Int. Ed.*, **45**, 2897.

23 Gasteiger, H.A. and Garche, J. (2008) Fuel cells. In *Handbook of Heterogeneous Catalysis*, 2nd edn (eds G. Ertl, H. Knözinger, F. Schüth, and J. Weitkamp), Wiley-VCH Verlag GmbH, Weinheim, p. 3081.

24 Qiu, J.M. and Wang, J.P. (2007) *Adv. Mater.*, **19**, 1703.

25 Ferreira, P.J., la O', G.J., Shao-Horn, Y., Morgan, D., Makharia, R., Kocha, S., and Gasteiger, H.A. (2005) *J. Electrochem. Soc.*, **152**, A2256.

26 Chen, S., Gasteiger, H.A., Hayakawa, K., Tada, T., and Shao-Horn, Y. (2010) *J. Electrochem. Soc.*, **157**, A82.

27 Ota, K. and Koizumi, Y. (2009) Platinum dissolution models and voltage cycling effects: platinum dissolution in polymer electrolyte (PEFC) and low-temperature fuel cells. In *Handbook of Fuel Cells – Fundamentals, Technology and Applications* (eds W. Vielstich, H.A. Gasteiger, and H. Yokokawa), John Wiley & Sons, Ltd, Chichester, vol. 5, p. 241.

28 Yu, P.T., Gu, W., Zhang, J., Makharia, R., Wagner, F.T., and Gasteiger, H.A. (2009) Carbon-support requirements for highly durable fuel cell operation. In *Polymer Electrolyte Fuel Cell Durability* (eds M.I.F.N. Büchi and T.J. Schmidt), Springer, New York, p. 29.

29 Reiser, C.A., Bregoli, L., Patterson, T.W., Yi, J.S., Yang, J.D.L., Perry, M.L., and Jarvi, T.D. (2005) *Electrochem. Solid State Lett.*, **8**, A273.

30 Kinoshita, K., Lundquist, J., and Stonehart, P. (1973) *J. Electroanal. Chem.*, **48**, 157.

31 Mathias, M.F., Makharia, R., Gasteiger, H.A., Conley, J.J., Fuller, T.J., Gittleman, C.J., Kocha, S.S., Miller, D.P., Mittelsteadt, C.K., Xie, T., Yan, S.G., and Yu, P.T. (2005) *Interface*, **14**, 24.

32 Darling, R.M. and Meyers, J.P. (2003) *J. Electrochem. Soc.*, **150**, A1523.

33 Greszler, T.A., Moylan, T.E., and Gasteiger, H.A. (2009) Modeling the impact of cation contamination in a polymer electrolyte membrane fuel cell. In *Handbook of Fuel Cells – Fundamentals, Technology and Applications* (eds W. Vielstich, H.A. Gasteiger, and H. Yokokawa), John Wiley & Sons, Ltd, Chichester, vol. 6, p. 728.

34 Makharia, R., Kocha, S., Yu, P., Sweikart, M.A., Gu, W., Wagner, F., and Gasteiger, H.A. (2006) *ECS Trans.*, **1** (8), 3.

35 Shao-Horn, Y., Sheng, W.C., Chen, S., Ferreira, P.J., Holby, E.F., and Morgan, D. (2007) *Top. Catal.*, **46**, 285.

36 Wagner, F.T., Yan, S.G., and Yu, P.T. (2009) Catalyst and catalyst-support durability. In *Handbook of Fuel Cells – Fundamentals, Technology and Applications*

(eds W. Vielstich, H.A. Gasteiger, and H. Yokokawa), John Wiley & Sons, Ltd, Chichester, vol. 5, p. 250.

37 Carter, R.N., Gu, W., Brady, B., Yu, P.T., Subramanian, K., and Gasteiger, H.A. (2009) Electrode degradation mechanisms studied by current distribution measurements. In *Handbook of Fuel Cells – Fundamentals, Technology and Applications* (eds W. Vielstich, H.A. Gasteiger, and H. Yokokawa), John Wiley & Sons, Ltd, Chichester, vol. 6, p. 829.

38 Yu, P.T., Gu, W., Makharia, R., Wagner, F.T., and Gasteiger, H.A. (2006) *ECS Trans.*, **3** (1), 797.

39 Gu, W., Carter, R.N., Yu, P.T., and Gasteiger, H.A. (2007) *ECS Trans.*, **11** (1), 963.

40 Perry, M.L., Patterson, T.W., and Reiser, C. (2006) *ECS Trans.*, **3** (1), 783.

41 Patterson, T.W. and Darling, R.M. (2006) *Electrochem. Solid State Lett.*, **9**, A183.